Iraqi Journal of Science, 2021, Vol. 62, No. 3, pp: 912-926
DOI: 10.24996/ijs.2021.62.3.22

ISSN: 0067-2904

A Study of Desertification Using Remote Sensing Techniques in Basra Governorate, South Iraq

Fadel Abbas Zwain*[1], Thair Thamer Al-Samarrai[1], Younus I. Al-Saady[2]
[1]Department of Geology, College of Science, Baghdad University, Baghdad, Iraq
[2]Iraqi Geological Survey (GEOSURV), Baghdad, Iraq

Received: 27/12/2019 Accepted: 9/7/2020

Abstract

Iraq territory as a whole and south of Iraq in particular encountered rapid desertification and signs of severe land degradation in the last decades. Both natural and anthropogenic factors are responsible for the extent of desertification. Remote sensing data and image analysis tools were employed to identify, detect, and monitor desertification in Basra governorate. Different remote sensing indicators and image indices were applied in order to better identify the desertification development in the study area, including the Normalized difference vegetation index (NDVI), Normalized Difference Water Index (NDWI), Salinity index (SI), Top Soil Grain Size Index (GSI) , Land Surface Temperature (LST) , Land Surface Soil Moisture (LSM), and Land Degradation Risk Index (LDI) which was used for the assessment of degradation severity .Three Landsat images, acquired in 1973, 1993, and 2013, were used to evaluate the potential of using remote sensing analysis in desertification monitoring. The approach applied in this study for evaluating this phenomenon was proven to be an effective tool for the recognition of areas at risk of desertification. The results indicated that the arid zone of Basra governorate encounters substantial changes in the environment, such as decreasing surface water, degradation of agricultural lands (as palm orchards and crops), and deterioration of marshlands. Additional changes include increased salinization with the creeping of sand dunes to agricultural areas, as well as the impacts of oil fields and other facilities.

Keywords: Desertification, Land Degradation, Basra , Image Indices

دراسة التصحر بإستخدام تقنيات التحسس النائي في محافظة البصرة، جنوب العراق

فضل عباس زوين*[1] ، ثائر ثامر السامرائي[1] ، يونس ابراهيم الساعدي[2]
[1]قسم علم الارض، كلية العلوم، جامعة بغداد، بغداد، العراق
[2]هيأة المسح الجيولوجي العراقية، بغداد، العراق

الخلاصة:

العراق عموما وجنوبه خصوصا يتعرض الى تصحر سريع وتدهور حاد للأراضي في القرن الاخير، العوامل الطبيعية والصناعية كلاهما سبب توسع ظاهرة التصحر. بيانات التحسس النائي ، وادوات تحليل المرئيات استخدمت لدراسة ومراقبة التصحر في محافظة البصرة ، مختلف دلالات التحسس النائي ومؤشرات المرئيات التي طبقت للحصول على افضل النتاج في تحديد تطور ظاهرة التصحر في منطقة الدراسة مثل دالة الاختلاف الطبيعي للنبات ،الاختلاف الطبيعي للمياه ، دالة التملح، دالة حجم الحبيبات لغطاء التربة ، وغيرها

*Email: f.zwain@gmail.com

باستخدام مرئيات لاندسات لسنوات 1973,1993،2013 والتي استعملت في مراقبة التصحر من خلال إمكانات التحسس النائي التحليلية ، النتائج تشير الى ان النطاق الجاف في محافظة البصرة شهد تغيرات بيئية كبيرة منها نقص المياه السطحيه ، تدهور الاراضي(بساتين النخيل والمحاصيل) ، تدهور الاهوار، زيادة التملح في الاراضي وكذلك زحف الكثبان الرملية باتجاه الاراضي الزراعية وحقول النفط وغيرها من المنشآت.

1. Introduction

Desertification phenomenon is one of the important environment problems in the world that leads to land degradation, which implies the lack of biological activities in land. This phenomenon happens following the decrease in vegetation and water in high temperature regions, the increase in salinity of soil and, the creeping of sand dunes to land. Desertification is considered as one of the most challenging threats to people's livelihoods and environment in the arid and semiarid regions. The desertification phenomena in Iraq was rapidly increased in the last decade due to the reduction of surface water by upstream countries and the decrease in precipitation, especially in central and southern parts of Iraq [1]. Monitoring and assessment of desertification are very important in terms of measuring and evaluating the degree of land degradation and the impact of actions undertaken. The movement of sand dune is considered as one of the most important features of desertification [2]. The rapidly increased desertification in Iraq has warranted much effort to define its causes and impacts [3].

Desertification in Iraq is distributed in large areas, most severely in southern Iraq. Basra Governorate has an area of 19070 km2, with a cultivable land of 233,8 km^2 that represents 2-12% of the total area [4]. The desert dominates in 70% of the land in Iraq, especially in the Mesopotamian and Sothern Desert , where the average participation rate is 50-200 mm annually [5].

1.1. Previous studies

AL-Hmedawy (2008) studied the geomorphological features and monitoring types and rates of land-surface changes reflected by remote sensing data in Haur Al-Hammar and adjacent areas in southern Iraq. He found that the main factor controlling the formation of landforms is human activities, followed by physical factors represented by water and wind. He also stated that, due to arid climate conditions, the effect of chemical factors is minor [6]. Suliman and Farhood (2015) studied sand dunes movement in Thi-Qar Governorate, to the northwest of the present study area, using image indices. They indicated decreased vegetation and increased bare land and sand dunes creeping [7]. Fadhil (2009) assessed land degradation and monitoring maps for some areas in north Iraq. He found significant risks of land degradation and diminution of water [8].

The main aims of this study are to assess desertification, determine land cover changes, recognize deterioration, and identify the effect of sand encroachment in this arid zone of Basra Governorate by using remote sensing techniques.

1.3. Study Area

The study area is located in the far southern Iraq, covering a large part of Basra Governorate, with a total area of 8395.85 Km^2 (Figure-1) situated between the Latitude (30°.55.57- 29°.53.56N) and Longitude (47°.59.15- 46°.37.55E). The northern part is located within the Mesopotamian plain and the southern part in the Sothern desert of Iraq, bounded in the north by the Euphrates river, in the north-west by Thi-Qar governorate, in the west by Al-Samawa Governorate, in the east by Khur Al-Zubair, and in the south by Kuwait. The area is characterized by a flat topography, from few meters to less than 50 m above sea level, and the presence of oil fields. The main marsh in the study area is Hor A-Hammar. The climate is warm to temperate with a dry and hot summer, especially in the desert [9]. The average humidity from May to October is less than 50%. This is associated with low precipitation in most months, increased soil erosion, and dust storms. The maximum temperature reaches more than 45 ºC in summer. According to the climate classification of Peltier [10], it could be concluded that the study area is under the influence of arid climate, characterized by long hot summer with occasional dust storms and short winter with limited and seasonal rainfall. The major portion of rainfall is received during the months of October to March.

1.4. Geological Setting

The study area lies within two physiographic provinces, the Southern Desert and the Mesopotamian Plain. Tectonically, the western desert is part of the Inner Platform and the Mesopotamia Foredeep is part of the Outer Platform [11]. The Southern Desert is characterized by a flat or rolling plain with occasional low hills dissected by shallow valleys and inland depressions. The Mesopotamian Plain is

characterized by a gradational feature of different origins that conferred an almost flat nature to the plain, which is dissected by rivers and marshes. There are three Geomorphological units recognized in the study area, these are; (i) units of alluvial origin, which include flood plains, and marshes, (ii) units of evaporation origin (inland and estuarine sabkha and gypcrete), (iii) units of aeolian origin [12]. Most structures of the study area do not appear on the surface or near surface. The most typical narrow elongated antifoams are the Zubair and Rumaila structures. Among other shorter and somewhat wider ones are the Nahr Umr, Rachi, Ratawi, and Luhais structures [13]. Jabal Sanam is the only exposure structure in the study area ; it is a unique domal structure penetrated in Al-Batin fan sediments [14]. The study area is characterized by poor rock exposures due to low relief and considerable Quaternary sediments cover. An exceptional case is Jabal Sanam, which is an outstanding high relief in the study area, where the oldest rocks are exposed. The studied sediments are described hereinafter in ascending stratigraphic order. The rocks sequence that is older than the Dibdibba Formation, exposed in Jabal Sanam vicinity, consists of 80 m of massive gypsum, mixed with boulders of silicified black dolomites and limestone. Dolerite with thin beds of limestone and marl exist on the top and bottom of the sequence. The stratigraphic description of this research is based on Yacoub (1992) [15].

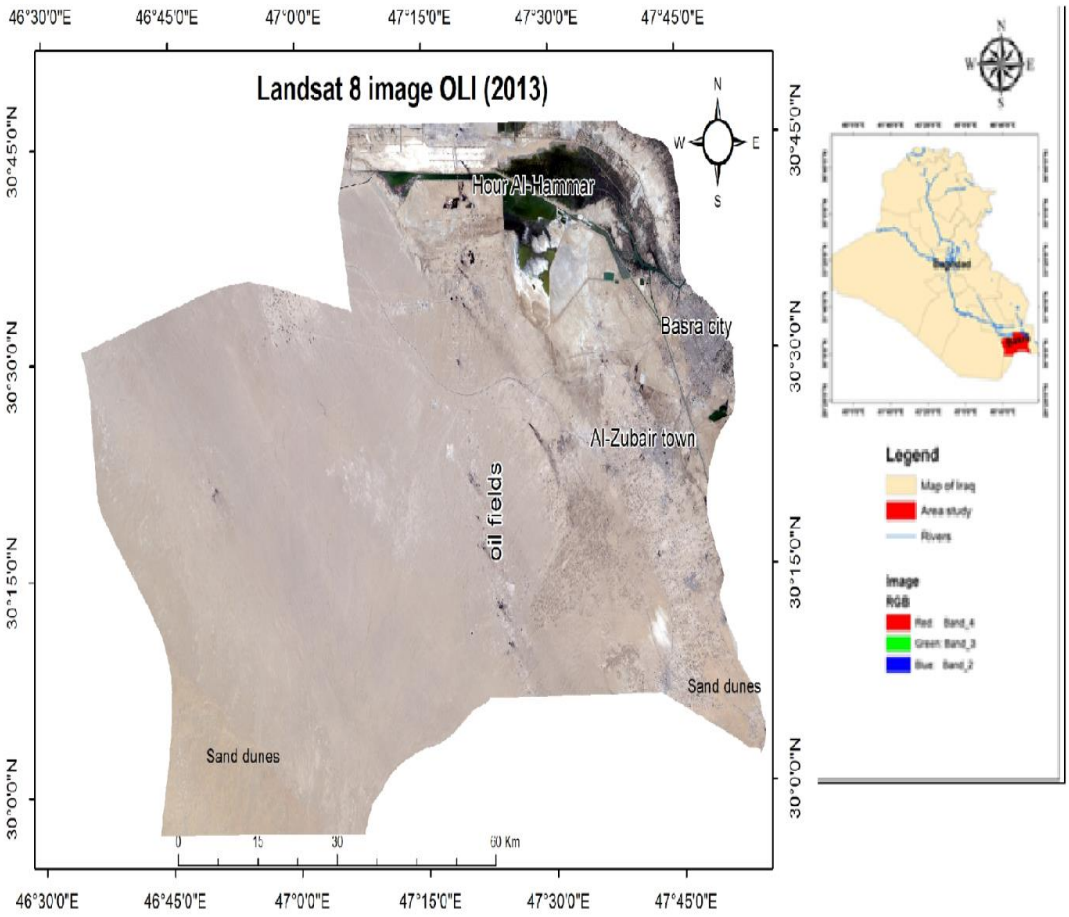

Figure 1- Location map of the study area

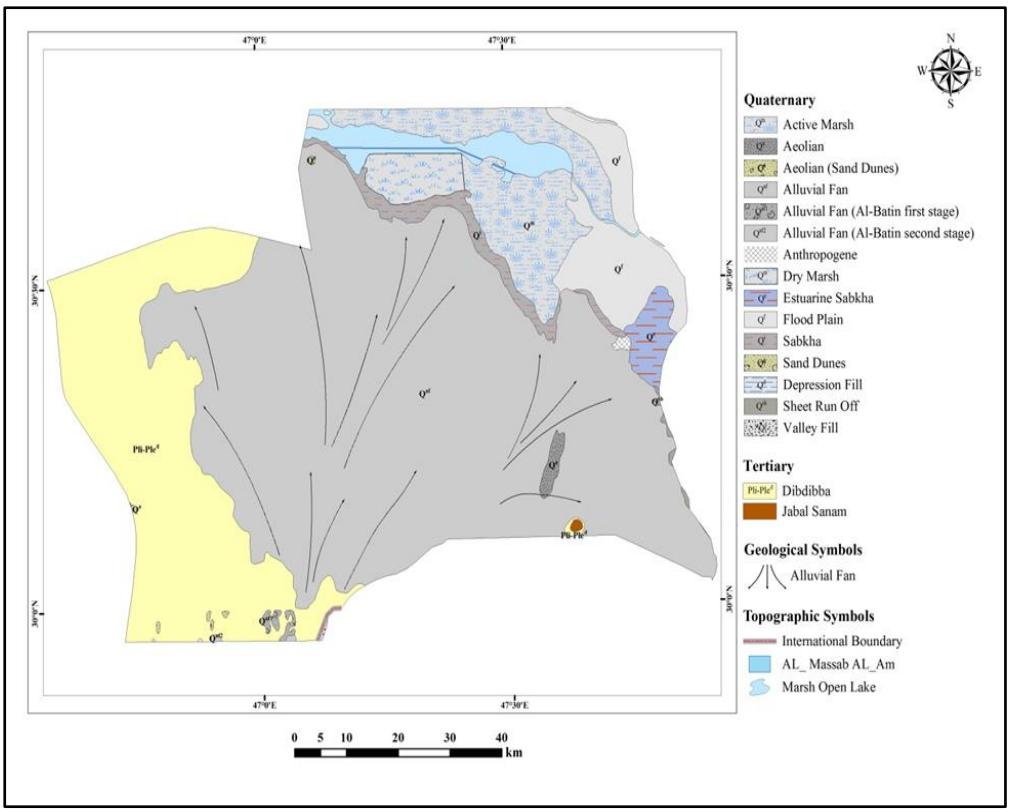

Figure 2- Geological map of the study area [15].

Dibdibba Formation (Pliocene-Pleistocene) is partly exposed on the eastern and southern sides of Jabal Sanam. This Formation is characterized by pebbly, medium to coarse, sand and sandstones with calcareous cement. The Quaternary sediments are divided according to origin, geomorphic position, and lithology. They include alluvial fan sediments, sheet run-off, (Holocene), estuarine sabkha, marsh, shallow depression and sabkha, flood plain, and Aeolian sediments (sand dunes and sand sheets).

2. Methodology

2.1. Data and Software

The principal data used in this paper were Satellite image (Landsat2-MSS in September 1973, Landsat TM -5 in September 1993, and Landsat8 OLI in October 2013) data downloaded from the USGS archive. All the satellite images were brought to the Universal Transverse Mercator (UTM) projection in zone 38N. Software such as ENVI V. 5.1 was used to calculate the radiometric calibration and atmospheric correction to calculate image indices and Arc Gis map 10.5 to classify image, and found area for each class and export map.

2.2. Image Processing

Each satellite image (1973, 1993, and 2013) was geo-referenced and ortho-corrected using the ENVI V. 5.1. The Landsat8 OLI image in October 2013 was classified using supervised classification in ENVI V. 5.1 software. Supervised classification was performed based on the ancillary data geological topographic map and previous studies , using the maximum likelihood methods. The accuracy of the classification was evaluated using a high-resolution image from Google Earth and other ancillary information. There are many factors that can affect the accuracy value of the resultant land use and land cover (LULC) map from the supervised classification, such as the characteristics of the satellite data, the scale of the study area, and the details in the LULC classes. Change detection and desertification monitring were achieved using image indices by ENVI V. 5.1 software. Desertification monitoring for the studied years was performed using the techniques described below.

Area of vegetation and sand dunes were calculated by using NDVI and GSI Indices, respectively. NDWI and SI indices, respectively, were used for water and salinity on surface. Previous indices determined the desertification for September 1973 , September 1993, and October 2013 , while GSI ,LST, and LSM indices were used only for 1993 and 2013 data because landsat TM-5 1973 neither has a blue band for GSI index nor a thermal band for LST and LSM indices.

- **Land use & Land cover**

Land use and land cover patterns were determined from the satellite image in ENVI V. 5.1 software and other geological data. The map was eventually exported in Arc map 10.6.

- **Normalized difference vegetation index**

In order to detect the surface area changes of vegetation cover in the image dates (1973, 1993 and 2013), the vegetation cover of the study area in each temporal image was extracted individually. NDVI value can be calculated from the ratio between the Red and NIR bands for the Landsat image data. It was used to monitor the aerial extension of the vegetation cover as well as the temporal change, using equation (1) [16]:

$$\boldsymbol{NDVI = \frac{(NIR - R)}{(NIR + R)}} \quad \ldots (\mathbf{1})$$

NDVI ranges from +1to -1, in Landsat MSS Band 2 is R (red), Band-3 NIR near infrared, in Landsat TM band-4 NIR, and R (red) band-3 while in Landsat-8 OLI NIR (band-5) and R (band-4).

- **Normalized Difference Water Index**

NDWI has been widely used to delineate surface water features using remote sensing. NDWI equation is used for MSS, TM, and Landsat 8 OLI images. Determination of surface water was achieved using the method of extracting thematic images from band ratios, according to equations (2) [17] and (3) [18].

$$\mathbf{NDWI\ for\ Landsat\ 8\ and\ TM5} = \frac{(\boldsymbol{\rho Green - \rho SWIR})}{(\boldsymbol{\rho Green + \rho SWIR})} \quad \ldots (\mathbf{2})$$

$$\mathbf{NDWI\ for\ MSS} = \frac{(\boldsymbol{\rho Green - \rho NIR})}{(\boldsymbol{\rho Green + \rho NIR})}. \quad .. (3)$$

ρGreen band 1 in MSS Landsat 5 , band 2 in TM and band 3 in Landsat 8 OLI.
ρSWIR band 5 in TM and band 6 in Landsat 8 OLI. ρNIR band 4 in Mss band.

- **Salinity index**

Soil salinization is one of the most important land degradation processes in arid and semi-arid regions that are characterized by high temperature and low precipitations during most parts of the year. Salinization, or rise of salt affected soils, is one of the common processes of soil degradation causing land desertification [19]. SI is an index that makes use of green and red bands, as shown in equation (4) [1]:

$$\boldsymbol{SI = \frac{(Green + Red)}{2}} \quad \ldots (\mathbf{4})$$

In Landsat TM, and MSS; Band2=green, Band3=red
Landsat 8 OLI can use SI as proposed by equation (5) [20]:

$$\boldsymbol{SI = \frac{(NIR * R)}{R}} \quad \ldots (\mathbf{5})$$

- **Top Soil Grain Size Index**

The grain size of topsoil characterizes soil texture and other physical properties. Consequently, the change in topsoil grain size can be effectively applied to monitor desertification by using remote sensing.
The GSI is calculated by using f equation (6) [21]:

$$\boldsymbol{GSI = \frac{R-B}{R+B+G}} \quad \mathbf{\ldots (6)}$$

R, B, and G represent red, blue, and green bands for the satellite image , respectively. Grain size index value is close to 0 in the vegetated regions and has a negative value for water bodies. GSI is not found by Landsat MSS 1973 because of the unavailability of the blue band.

- **Land Surface Temperature**

The satellite TIR sensors measure emitted radiance from top atmosphere which derived brightness temperatures using Planck's law [22].
For images, the digital number (DN) is converted to an at-sensor spectral radiance (Lλ) using equation (7) [23]:

$$\boldsymbol{L_\lambda = M_L Q + A_L} \quad \mathbf{\ldots (7)}$$

where ML is band specific multiplicative (from the metadata). Q cal is a quantized and calibrated standard (from the DN value of pixel). AL is band specific additive (from the metadata).
Brightness temperature (BT) can be calculated from converting the thermal infrared bands using the following equation (8) [23]:

$$BT = \frac{K_2}{Ln[\left(\frac{k_1}{L_\lambda}\right)+1]} - 273.15 \quad \text{… (8)}$$

where K1 and K2 are thermal constants which can be found in the metadata file existing with the satellite image. The results are expressed in ◦C, zero in Kelvin scale which is approximately equal to (-273.15 C◦).
Land surface temperature is calculated by equation (9) [24]:

$$LST = \frac{BT}{[1+\{\left(\frac{\lambda BT}{\rho}\right) ln\varepsilon\lambda\}]} \quad \text{… (9)}$$

where λ is the wavelength of the emitted radiance, for which the peak response and the average of the limiting wavelengths are achieved at 11.5.
Land surface emissivity (ε) is calculated by equation (10) [25]:

$$\varepsilon = 0.004 * Pv + 0.986 \quad \text{... (10)}$$

The proportional vegetation (Pv) is calculated from the NDVI index, as in equation (11)

$$Pv = (\frac{NDVI-NDVI_S}{NDVI_V-NDVI_S})^2 \quad \text{… (11)}$$

where NDVIs is the minimum value and NDVIv is the maximum value in NDVI index.
Land surface temperature was not calculated for Landsat MSS 1973 because the thermal band was not available.

- **Land Surface Soil Moisture**

Soil moisture index can be found from the land surface index, land surface temperature, and NDVI through a relationship called the dry edge and wet edge, which is calculated using equation (12) [26]:

$$SMI = (LSTmax - LST)/ (LSTmax - LSTmin) \quad \text{… (12)}$$

where $LSTmax$ and LSTmin are, respectively, the maximum and minimum surface temperatures for a given NDVI and LST. LST of a pixel for a given NDVI is extracted from the provided remote sensing data. $LSTmax$ and LSTmin are calculated using equations (13) and (14), respectively [25]:

$$LSTmax = a1 * NDVI + b1 \quad \text{… (13)}$$

$$LSTmin = a2 * NDVI + b2 \quad \text{… (14)}$$

where $a1$, $a2$, $b1$, and $b2$ are the empirical parameters obtained by the linear regression. a presents the slope and b presents the intercept, defining both warm and cold edges of the data, respectively. Land surface soil moisture was not calculated for Landsat MSS 1973 because LST was not available.

- **Assessment of Degradation Severity by LDI**

LDI is a value ($0 \leq LDI \leq 1$) that represents the degree of degraded land, which can be found by equation (15) [27]:

$$LDI=\sum_{i=1}^{n} PCi^{-q} \quad \text{… (15)}$$

C_i is the rank for the land, P is the percentage for the land having a rank, n is the number of indicators, and q is the weighting that exponents for each indicator.
Depending on the previous studies, factors of desertification severity which play important roles in the assessment were determined by four indicators, namely the vegetation, sand dunes drifting, population pressure, and annual desertification rate.

Table 1- The four indicators used in the assessment of land degradation severity with their weights of effectiveness [27].

Indicators	Severity level				Weight
	I – severe	II – high	III – medium	IV – low	
Vegetation cover (%)	<10	10–25	25–40	>40	0.40
Drifting sand coverage (%)	>65	15–65	5–15	<5	0.25
Annual desertification rate (%)	>5	2–5	1–2	<1	0.15
Population pressure (%)	>50	30–50	0–30	–30–0	0.20

Vegetation cover area was found from the NDVI index, drifting sand from GSI index, population

pressure area from Landsat image, and annual desertification from annual vegetation change with the increase in sand drift and population.

3. Results and Discussion

LULC classification of the study area is derived from the supervised classification using ENVI V. 5.1 software, depending on Landsat images as well as previous maps.

The number of main classes was four with two subsidiary classes. The main area was represented by the barren land (5178,13 km^2), as shown in Table-2 , forming 62% of the total area. Two subsidiary classes were identified within the barren land class. The first subsidiary class was the sand sheet and sand dunes (2390,81 km^2 , 28%), whereas the second was the dry salt flat (284,89 km^2 , 3%). The barren land class with its two subsidiary classes represents 93% of the total area. This implies that the major part of the area was desert. To monitor and assess the desertification change in previous years, the values of the indices of NDVI, GSI, NDWI, SI, LST and LSM were calculated and the map was eventually exported by Arc Map 10.5. Sand dunes and saline land showed increased LST and GSI and decreased LSM values. An increased heat emission was observed in the map of LST 2013s compared with the map 1993s, as shown in Figure-9. Most of the area had a high LST value, with a high GSI value in some area. Also, the SMI value was decreased in the area during the same year. The area of vegetation cover increased by about 154.80 km^2 from 1973s to 1993s , with a decrease of about -297.34 km^2 from 1993s to 2013s. Water body area decreased gradually by 125.68 km^2 from 1973s to 1993 and by 72.17 km^2 from 1993s to 2013s. The area of saline land increased by 3.15 km^2 from 1973s to 1993s and by 166.91 km^2 in 1993s to 2013s, as shown in Figure-3, Figure-4, Table-2, and Table-3. The percentage of vegetation area to the total area studied was about 2.6% in 1973s, while it was increased to 4.52% in 1993s, then to 0.87% in 2013s. all period severe I level degradation depend on Table-1. Percentage of sand dunes showed values of 10% (medium III level) in 1993s and 29% (high II level) in 2013s . The percentage values of urban area were 2.34% and 4.13% in 1993 and 2013, respectively. LDI value depends on the changes in urban, vegetation and sand dune areas as well as annual desertification rate. The degree of land degradation showed an increase in 2013s.

Table 2-Areas in km^2 of vegetation , water, and dry salt flat surfaces in 1973, 1993, and 2013.

Year	Dry salt flat	Vegetation	Water
1973	114.82	213.19	356.32
1993	117.98	367.99	230.64
2013	284.89	70.65	158.47

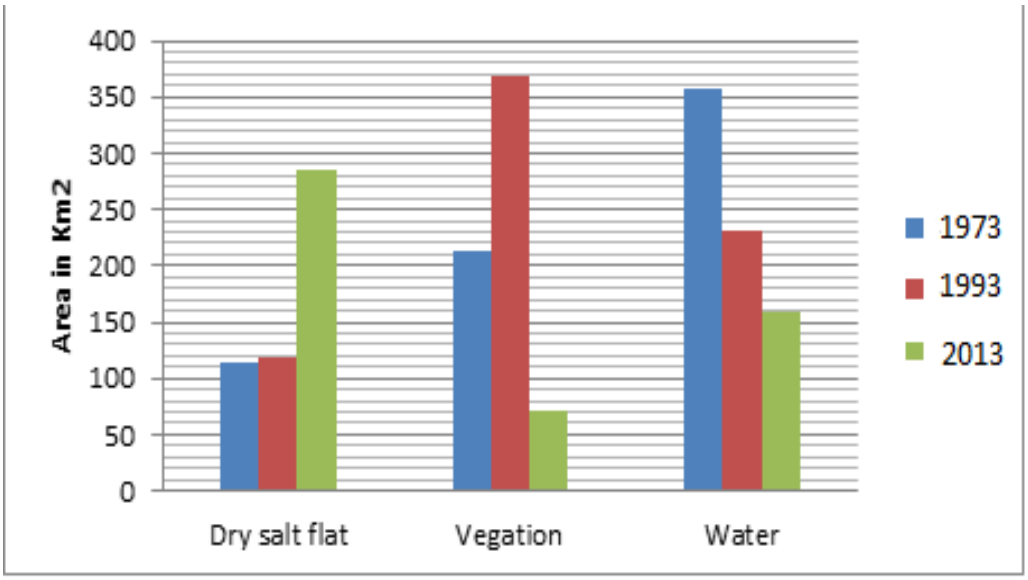

Figure 3- Changes in saline, vegetation, and water areas in 1973,1993, and 2013.

3.1. Classification of the Study Area

The six classes of land showed various area values (Figure-5, Table-3). The largest class which dominated the area is that of the bare land that contained sandstone and sediment along with small areas of vegetation .

3.1.1. Agricultural Land:

Agricultural land in Basra Governorate was classified into three types, namely palm trees, barley, and wheat. Palm trees are concentrated around the banks of the rivers, whereas barley and wheat are distributed in the south and east of the study area, which are irrigated by ground water. The area of agricultural land is very small compared with that of the other classes, with a percentage of 1%. The coverage area of LULC classes is shown in Figure- 4.

3.1.2. Water

This class includes any water body in the surface, such as rivers, linear water bodies, and lakes. The map illustrates two sources for water, which are represented by a lake (Hour Al-Hammar) and a river (Shatt Al-Arab). The collective area of all water bodies in the study area is displayed in Figure-5, with a percentage of 2%.

3.1.3. Urban land

The land that represents human activities is covered by built areas inside or outside the cities, occupied by concrete constructions, houses, and roads. Figure-5 shows that the urban land is mainly represented by Basra city and Zubair town as well as the oil fields. There are also constructions and buildings outside cities. The percentage of the urban land in the study area is 4%.

3.1.4. Bare Land

In the study area, the bare land was composed of soil, sediment (sand and gravels), sandstone and salt areas, while vegetation, if present, occupied widely spaced areas such as shrub lands [28].. The percentage of the bare land in the study area is 62%.

3.1.5. Dry Salty Flat Land

When surface or ground water evaporates and unorganized irrigation is practiced, increased concentrations of salts appear at the surface. The map shows that the salty flat land is present near Hour Al-Hammar and at the agricultural lands. The percentage of the dry salty flat land in the study area is 3%.

3.1.6. Sand Sheets and Sand Dunes

Sand sheets and dunes constitute one type of barren land according to Anderson *et al.*, (1976) [28]. A sand dune develops in dry and semi dry lands and reflects land degradation because it contains a high percentage of quartz and a low content of organic matter, rendering it unsuitable for agricultural uses. Field of dunes was distributed in the south and south-east parts of the study area. Sand dunes take the shape of barchans that consist mainly of quartz grains [11]. Sand sheets cover extreme areas with a slight thickness. The percentage of sand sheets and dunes in the study area is 28%.

Table 3- Area of each land use and land cover class.

Class	**Area** (km^2)
Urban Land	336
Agricultural Land	70,65
Sand Sheet & Sand Dunes	2390,81
Dry Salt Flat	284,89
Water	158,47
Bare Land	5178,13

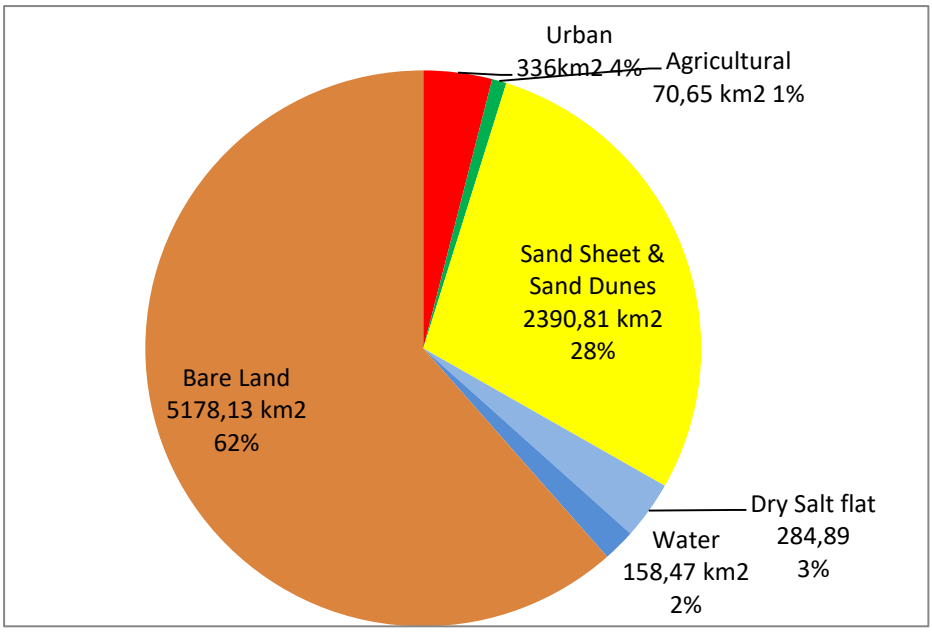

Figure 4- Pie chart showing the coverage area of LULC classes.

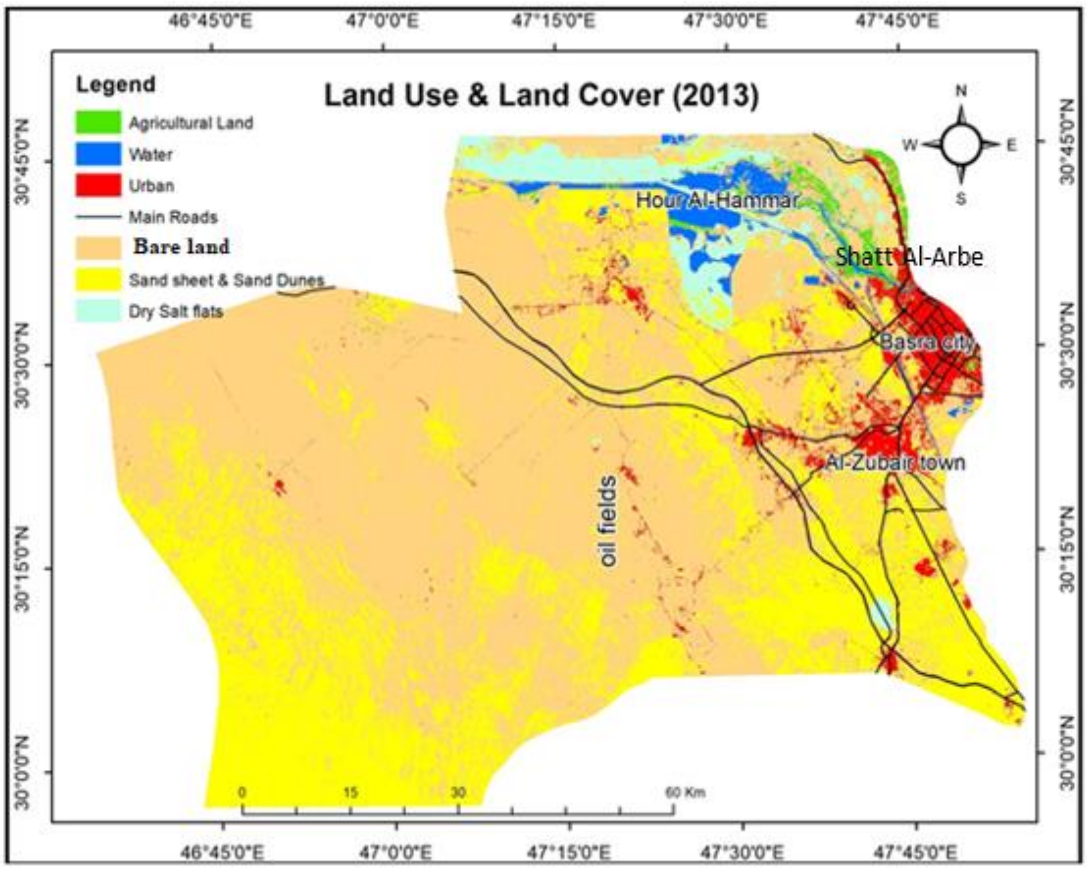

Figure 5- Map showing land use and land cover classes.

3.2. Desertification indices

3.2.1. NDVI Index

NDVI index was used to refer to vegetation land for the three specified time periods (Figure-6 A:1973 , B:1993, and C:2013). The highest NDVI value appeared in 1993s , due to the increase in the area of cultivated lands , whereas it decreased in 2013s because of the neglecting of agriculture in recent years.

3.2.2. NDWI

The water area, according to the normalized difference water index, showed decreased values from 1973s to 2013s . This indicates a reduction in water resources in the three periods (Figure-7 A:1973, B:1993, C:2013).

3.2.3. SI Index

Salinity index value increases when salts concentration on the surface soil increases. In the three periods form 1973 to 2013, the index value showed an increase (Figure-8) A:1973, B:1993, C:2013), especially in 2013s because of reduced water resources and increased evaporation.

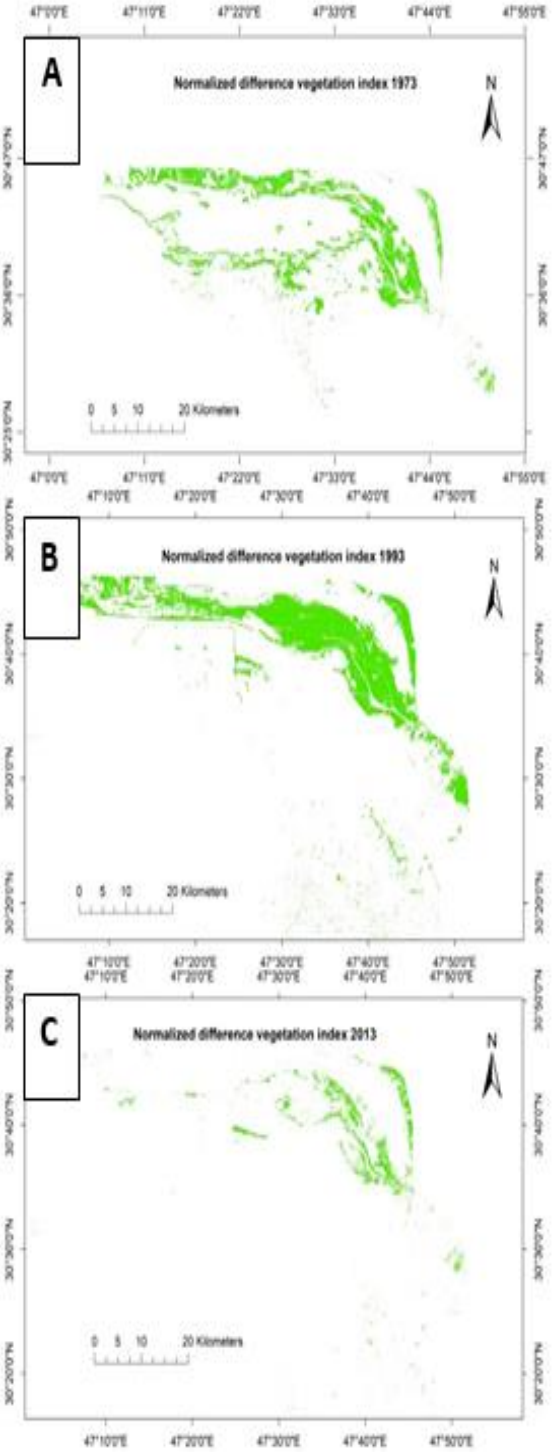

Figure 6- NDVI in three period. (A:1973, B:1993 & C:2013)

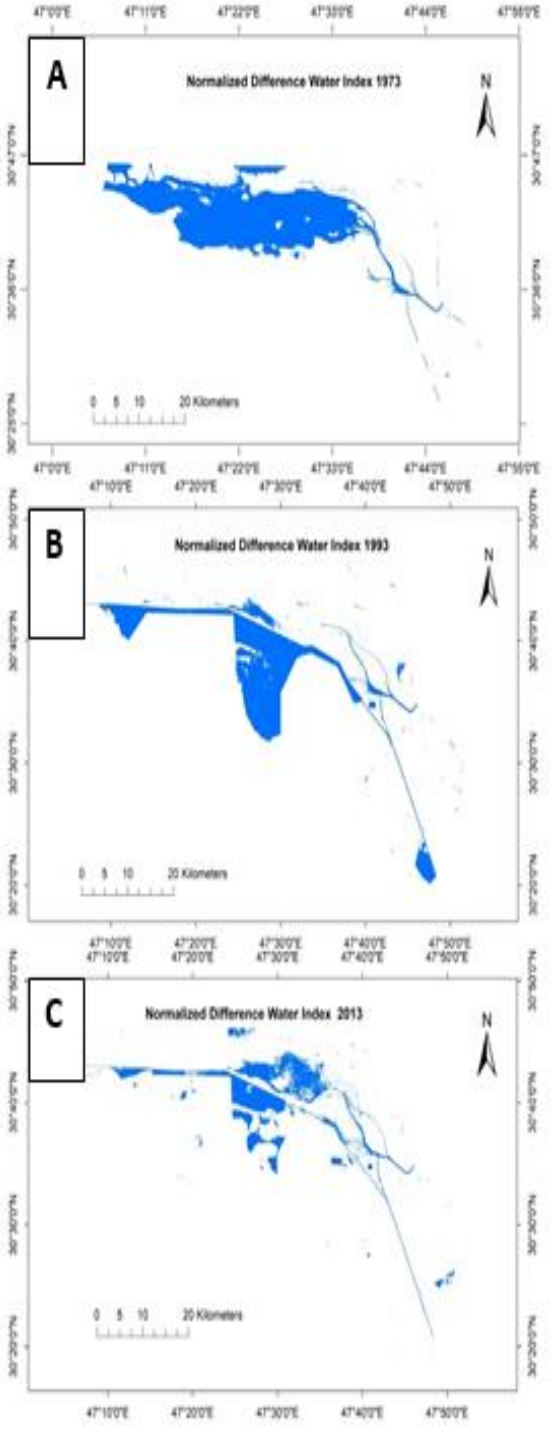

Figure 7- NDWI in three period. (A:1973, B:1993 & C:2013)

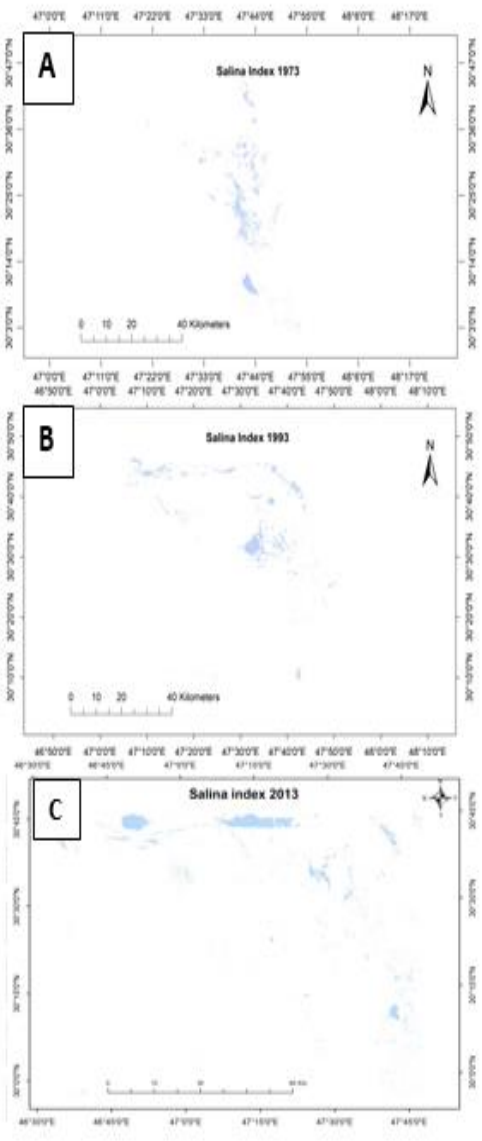

Figure 8- SI in three period (A:1973, B:1993 & C:2013)

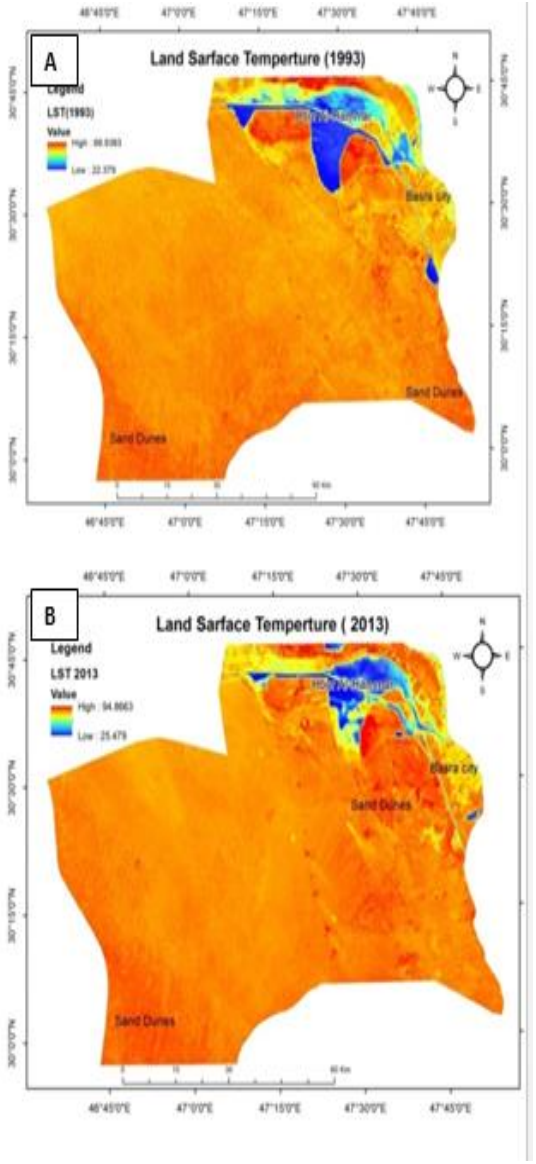

Figure 9- land surface temperature maps (A:1993s & B:2013s)

3.2.4. Land Surface Temperature Index

A region of high land surface temperature refers to dry lands, such as that shown by sandy lands or dry farm lands in the map of 2013s in Figure-9, which demonstrates increased values of the index and area of high temperature, which results in decreased water surfaces.

3.2.5. Land Surface Soil Moisture Index

Soil moisture index value increases with the increase in areas of water bodies, irrigation farmlands, wet sand, and high coverage vegetation, while it decreases with the increase in the area of dry sandy land. The map of 1993s in Figure-10A shows regions of high index values, while those illustrated in the map of 2013s in Figure- 10B are greatly reduced. This indicated a decrease in water content of soil in the map of 2013s.

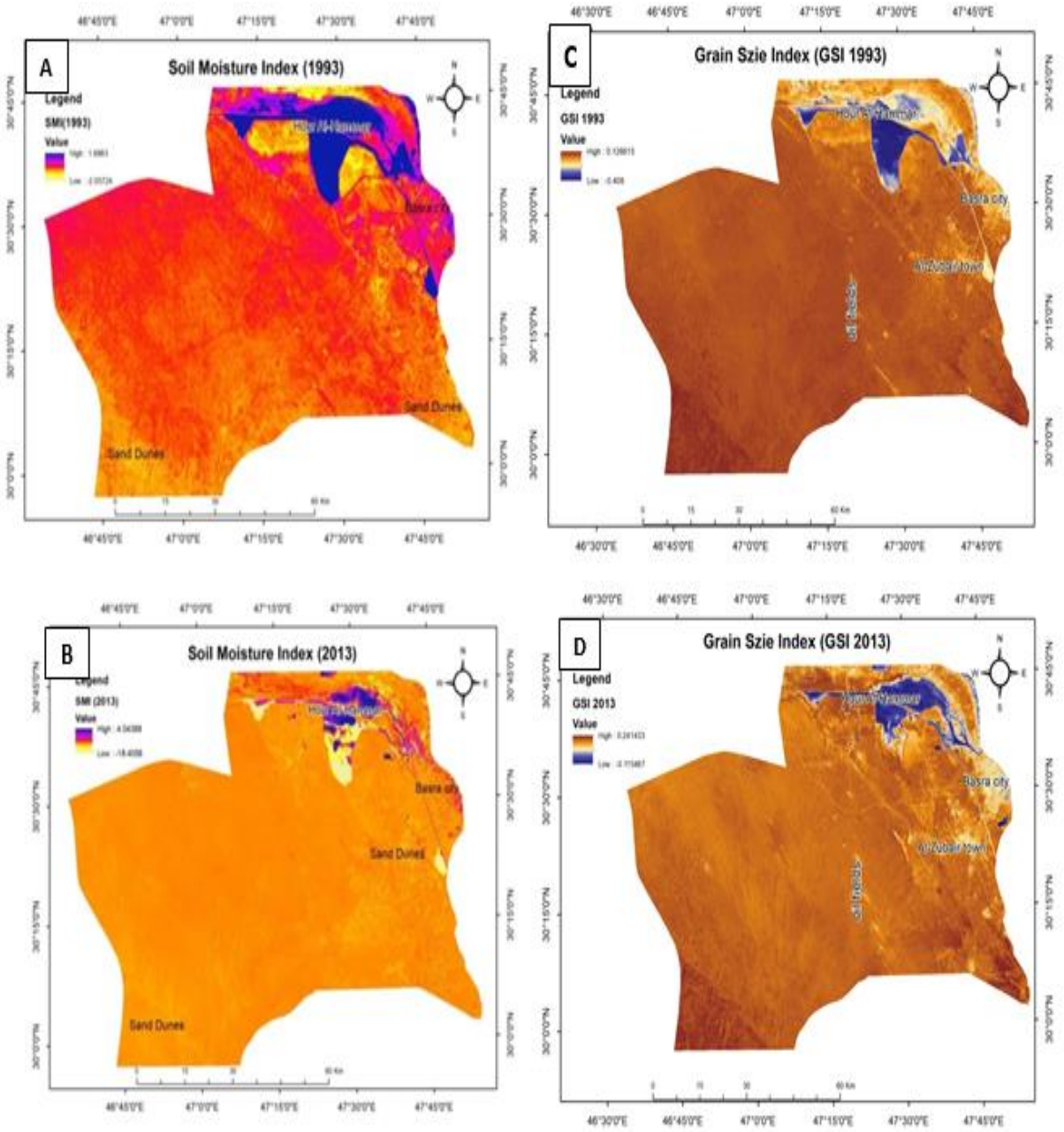

Figure 10- Maps indicating soil moisture index values (A:1993s , B: 2013s) and GSI index values (C: 1993, D: 2013).

3.2.6. Top Soil Grain Size Index

The dark area of the map of 2013s in Figure-10D refers to high GSI value, reflecting sandy land, dry soil, and coarse grain size. The value showed an increase toward the south-east and south-west as compared to the north (Hour-Al-Hammar and farm lands).

3.2.7. Land Degradation Index

Annual desertification rate in 1993 was 4%, while that in 2013 was 21%, depending on the annual change in total vegetation area, as shown in Table -4 and (Figure-11).

Table 4- Percentage and change in area of indicators.

Vegetation						
Total Area (km2)	Area in1993 to Vegetation	Percentage area to Vegetation in 1993s	Area in 2013 to Vegetation	Percentage area to Vegetation in 2013s	Deference 1993-2013	change rate km^2 year-1
8129.41	367.99	4.52	70.65	0.87	297.34	14.86
Sand dunes						
Total Area (km2)	Area in1993 to Sand dunes	Percentage area to Sand dunes in1993	Area in 2013 to Sand dunes	Percentage area to Sand dunes in1993	Deference 1993-2013	change rate km2 year-1
8129.41	841.44	10	2390.81	29	-1549.36*	-77.46*****
Urban						
Total Area (km^2)	Area in1993 to Urban	Percentage area to Urban in1993	Area in 2013 to Urban	Percentage area to Urban in1993	Deference 1993-2013	change rate km^2 year-1
8129.41	190.62	2.34	336	4.13	-145.38	-7.26

*****Negative signs refer to increased indicator value, which mean increase land degradation risk.

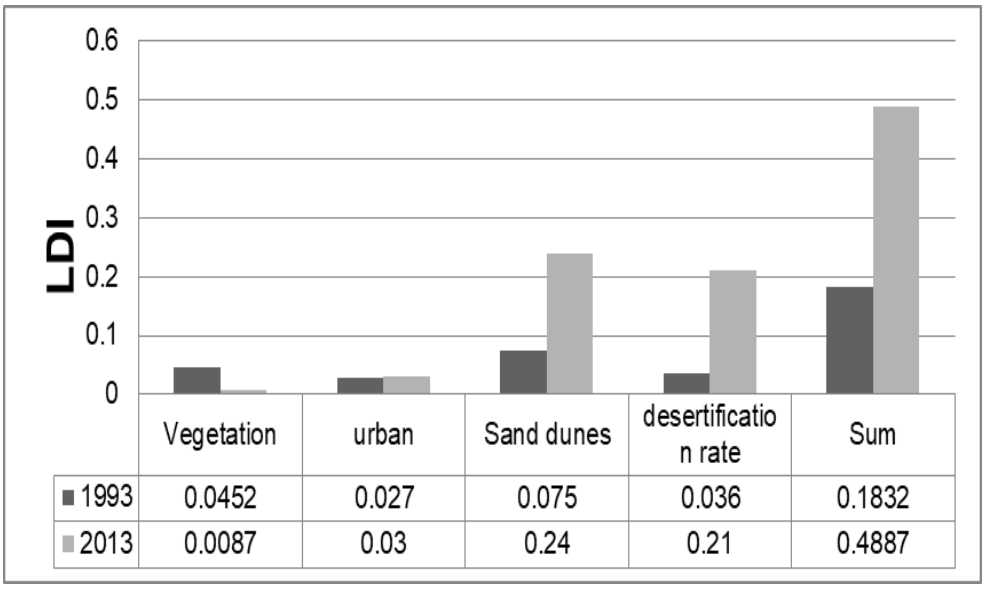

Figure 11- Land degradation index for 1993-2013s

4. Conclusions

The results of this study confirm the usefulness of image indices for characterizing, detecting, and assessment of desertification in Basra Governorate, South Iraq.

The identified classes of the land were sand sheet and sand dunes, dry salt flat land, bare land, urban land, water, and agricultural land. The dominant class was the bare land while the smallest area belonged to the agricultural land class.

Most land areas suffered from desertification. The bare land was mainly dominated by soil, sediment (sand and gravels), sandstone and salt land sand sheet or dunes, salt flat and saline soils. Long term monitoring of the study area using image indices can display noticeable changes. Vegetation cover monitoring from1993 to 2013s using NDVI index showed a decrease in this parameter, which attributed mainly to decreased aquatic vegetation within Hor Al-Hammar as well as the decrease in agricultural lands.

Monitoring salinity in land surfaces from 1973 to 2013s using SI index showed increased salt areas because of the decreased water resources, as indicated by the NDWI value in the same year, as well as the increased evaporation.

Land surface temperature index increased in some areas of sandy or dry farm lands, with decreased water content which reflects high temperature. Desertification increases with the increase in these indices, in map 2013s increase area of high index than map 1993s.

Soil moisture index, opposite to the index of surface land temperature, showed an increase, leading to a decreased desertification, that high water content in area of soil moisture in map 2013s decreases area compare with 1993s.

When the value of GSI index of surface soil increases, it reflects dominance of dry soil sand and coarse grain soil. As shown in the map of 2013s, a very high value was recorded in the areas toward Hour-Al-Hammar and the farm lands because of creep sand dunes from desert to ward oil fields and agricultural areas.

Water body percentage was 4.38% in 1973s, 2.8% in 1993s, and 1.9% in 2013s, reflecting a gradual decrease. Pollution through those 40 years was one of the main reasons for desertification and land degradation.

The value of land degradation risk index showed a very high increase in 2013s compared with that in 1993s due to the increased changes in the values of the other indicators.

5. References

1. Othman, Arsalan A., Younus I. Al-Saady, Ahmed K. Al-Khafaji, and Richard Gloaguen. **2014**. "Environmental Change Detection in the Central Part of Iraq Using Remote Sensing Data and GIS." *Arabian Journal of Geosciences* **7**(3): 1017–28.
2. Cornet, Antoine. **2002**. "Desertification and Its Relationship to the Environment and Development: A Problem That Affects Us All." *Wo Rld Su Mm It on Sust Ain Able Develop Me Nt* 100.
3. Al-Saady, Younus I., Al-Obaydi, Manal M. and Ahmed, Mousa A. **2013**. Monitoring of aeolian deposits and environmental changes detection of ali al-gharbi area, south east iraq, using remote sensing and gis techniques." *Iraqi Bulletin of Geology and Mining*, **9**(2): 47-79.
4. Farg, S.G.and Mohammed, T.K. **2017**. Desertifcation , salinity and economic impacts in Iraq with Basra governorate. *Alqtsad Alkaliji in arabic*, p. 33.
5. Ali, H. Z. and Abod, R. A. **2009**. A study Desertifcation phenomenon in central Iraq uesing remote sensing techniques. *Scientific Conference* (p. 43). Wasit: University of Wasit.
6. Al-Hmedawy, H. D. **2008**. Geomorphological study of Haur Al-Hammar and adjacent area southern Iraq. Ph.D. Thesis, College of Science, University of Baghdad, 170p.
7. Suliman, A. A. and Farhood , A.F. **2015**. Monitoring the Movement of Sand Dunes in Thi Qar Governorate Using Some Spectral Indices. *International Journal of Scientific Engineering and Research (IJSER)*, pp. ISSN (Online): 2347-3878.
8. Fadhil , A. M. **2009**. "Land Degradation Detection Using Geo-Information Technology for Some Sites in Iraq". *Journal of Al Nahrain University-Science* (JNUS), **12**(3): 94-108.
9. Kottek, M., Grieser, J., Beck, C., Rudolf, B., & Rubel, F. (2006). World map of the Köppen-Geiger climate classification updated. *Meteorologische Zeitschrift*, **15**(3): 259–263.
10. Peltier, Louis C. **1950**. "The Geographic Cycle in Periglacial Regions as It Is Related to Climatic Geomorphology." *Annals of the Association of American Geographers*, **40**(3): 214–36.
11. Fouad, S. F. 2010. "Tectonic Map of Iraq. Scale 1:1,000,000, 3rd, Ed.; GEOSURV: Baghdad, Iraq."
12. Sissakian, V. K. and F. A. Ibrahim. **2005**. *Geological Hazards in Iraq, Classification and Geographical Distribution,Scale1:1000000. GEOSURV.Baghdad, Iraq. Report No.2876.*
13. Buday, T. and S. Z. Jassim. **1980**. "Regional Geology of Iraq: Vol. 1." *Stratigraphy and Paleogeography, Iraq State Organization for Minerals, Baghdad, 445pp*.
14. Al-Naqib, K. M. 1970. "Geology of Jabal Sanam, South Iraq." *Journal of the Geological Society of Iraq*, **3**(1): 9–36.
15. Yacoub, S. Y. **1992**. *The Geology of AL-Basrah , Abadan, Bubyan Quadrangles Sheets NH-38-8,NH-39-5, & NH-39-9, Scale 1:25000. GEOSURV, Baghdad, Iraq.* Baghdad
16. Rouse, J. W., Hass, R. W., Schell, J. A., Deering, D. W., and Harlan, J. C. **1974**. Monitoring the

vernal advancement and retrogradiation (green wave effect) of natural vegetation. NASA/GSFCT Type III Final Report, Greenbelt, MD, USA.

17. Ji, L., Li Zhang, and B. Wylie. **2009**. *Analysis of Dynamic Thresholds for the Normalized Difference Water Index*. Vol. 75.

18. El-Asmar, Hesham M., Mohamed E. Hereher, and Sameh B. El Kafrawy. **2013**. "Surface Area Change Detection of the Burullus Lagoon, North of the Nile Delta, Egypt, Using Water Indices: A Remote Sensing Approach." *The Egyptian Journal of Remote Sensing and Space Science*, **16**(1): 119–23.

19. Sentis, I. **1996**. "Soil Salinization and Land Desertification." *Soil Degradation and Desertification in Mediterranean Environments. Logroño, Spain, Geoforma Ediciones* 105–29.

20. Abbas, A. and Khan, S. **2007**. Using Remote Sensing Techniques for Appraisal of Irrigated Soil Salinity. In: Oxley, L. and Kulasiri, D., Eds., MODSIM **2007** International Congress on Modelling and Simulation, Modelling and Simulation Society of Australia and New Zealand, December 2007, 2632-2638.

21. Xiao, J., Yanjun Shen, R. Tateishi, and W. Bayaer. **2006**. "Development of Topsoil Grain Size Index for Monitoring Desertification in Arid Land Using Remote Sensing." *International Journal of Remote Sensing*, **27**(12): 2411–22.

22. Dash, P., Göttsche, F. M. and Olesen, F. S. **2002**. Potential of MSG for surface temperature and emissivity estimation: considerations for real-time applications. *International Journal of Remote Sensing*, **23**(20): 4511-4518.

23. Walawender, J. p., Szymanowski, M., Hajto, M. J., Bokwa A. 2014. " Land syrface temperature patterns in the urban agglomeration of Krakow (Poland) mderived from Landsat-7/ETM+ data", *Pure and Applied Geophysics*, **171**(6): 913–940.

24. Stathopoulou M. and Cartalis C. **2007**. " Daytime urban heat islands from Landsat ETM+ and Corine land cover data: An application to major cities in Greece" , *Solar Energy*, **81**(3): 358-368.

25. Parida, B.R.; Collado, W.B.; Borah, R.; Hazarika, M.K. **2008**. Samarakoon, L. Detecting Drought-Prone Areas of Rice Agriculture Using a MODIS-Derived Soil Moisture Index. *GIsci. Remote Sens*., **45**: 109–12.

26. Zhang, D., Tang, R., Zhao, W., Tang, B., Wu, H., Shao, K. and Li, Z. L. **2014**. Surface soil water content estimation from thermal remote sensing based on the temporal variation of land surface temperature. *Remote Sensing*, **6**(4): 3170-3187.

27. Liu, Y., Goa. J. and Yang, Y. **2003**. "A holistic approach towards assessment of severity of land degradation along the great wall in northern Shaanxi Province, China". *Environmental Monitoring and Assessment*, **82**: 187–202.

28. Anderson , J.R. **1976**. A land use and land cover classification system for use with remote sensor data (Vol.964).US Government Printing Office.